Heliyon 9 (2023) e20466

Contents lists available at ScienceDirect

Heliyon

journal homepage: www.cell.com/heliyon

Cu_2O/Fe_3O_4/UiO-66 nanocomposite as an efficient fenton-like catalyst: Performance in organic pollutant degradation and influencing factors based machinelearning

Thi Thanh Nhi Le [a,b], Hai Bang Truong [c,d], Le Thi Hoa [e], Hoang Sinh Le [f], Thanh Tam Toan Tran [g], Tran Duc Manh [h], Van Thuan Le [a,b], Quang Khieu Dinh [e,**], Xuan Cuong Nguyen [a,b,*]

[a] Center for Advanced Chemistry, Institute of Research and Development, Duy Tan University, 03 Quang Trung, Da Nang, Viet Nam
[b] Faculty of Natural Sciences, Duy Tan University, 03 Quang Trung, Da Nang, Viet Nam
[c] Optical Materials Research Group, Science and Technology Advanced Institute, Van Lang University, Ho Chi Minh City, Viet Nam
[d] Faculty of Applied Technology, School of Technology, Van Lang University, Ho Chi Minh City, Viet Nam
[e] University of Sciences, Hue University, 77 Nguyen Hue, Hue, Viet Nam
[f] VN-UK Institute for Research and Executive Education, University of Danang, Danang city, Viet Nam
[g] Institute of Applied Technology, Thu Dau Mot University, Thu Dau Mot city, Viet Nam
[h] University of Danang, University of Science and Education, Da Nang, Viet Nam

ARTICLE INFO

Keywords:
Cu_2O
Fenton-like reaction
Machine learning
Reactive blue 19
UiO-66
Fe_3O_4

ABSTRACT

The persistent presence of organic pollutants like dyes in water environment necessitates innovative approaches for efficient degradation. In this research, we developed an advanced hybrid catalyst by combining metal oxides (Cu_2O, Fe_3O_4) with UiO-66, serving as a heterogeneous Fenton catalyst for for efficient RB19 breakdown in water with H_2O_2. The control factors to the catalytic behavior were also quantified by machine learning. Experimental results show that the catalytic performance was much better than its individual components ($P < 0.05$ & non-zero 95% C.I). The improved catalytic efficiency was linked to the occurrence of active metal centers (Fe, Cu, and Zr), with Cu(I) from Cu_2O playing a crucial role in promoting increased production of $HO^{\bullet}$. Also, UiO-66 served as a catalyst support, attracting pollutants to the reaction center, while magnetic Fe_3O_4 aids catalyst recovery. The optimal experimental parameters for best performance were pH at 7, catalyst loading of 1.6 g/L, H_2O_2 strength of 0.16 M, and reaction temperature of 25 °C. The catalyst can be magnetically separated and regenerated after five recycling times without significantly reducing catalytic activity. The reaction time and pH were ranked as the most influencing factors on catalytic efficiency via Random Forest and SHapley Additive exPlanations models. The findings show that developed catalyst is a suitable candidate to remove dyes in water by Fenton heterogeneous reaction.

* Corresponding author.Center for Advanced Chemistry, Institute of Research and Development, Duy Tan University, 03 Quang Trung, Da Nang, Viet Nam.
** Corresponding author.
E-mail addresses: Truonghaibang@vlu.edu.vn (H.B. Truong), dqkhieu@hueuni.edu.vn (Q.K. Dinh), nguyenxuancuong4@duytan.edu.vn (X.C. Nguyen).

https://doi.org/10.1016/j.heliyon.2023.e20466
Received 13 September 2023; Received in revised form 26 September 2023; Accepted 26 September 2023
Available online 27 September 2023

1. Introduction

Water contamination due to toxic organic compounds released from the production process and using dyes, pesticides, and antibiotics has been a severe environmental problem because water is crucial for living creatures [1–3]. Numerous methods like adsorption, advanced oxidation processes (AOPs, like photocatalysis, Fenton reaction), membrane filtration, osmosis, and biodegradation are used to treat organic compounds in wastewater [4–9]. Among them, the advantage of AOPs in water treatment is that the reactants are relatively cheap, readily available, non-toxic, and easy to use [10]. Furthermore, the organic pollutants (OPs) can be converted to CO_2, H_2O, and inorganic ions, or partially decomposed to new biodegradable substances by hydroxyl radicals $HO^{\bullet}$ generated from the Fenton reaction [11].

In recent years, the Fenton catalyst system has been studied intensely and developed widely worldwide. This system not only involves the classical Fenton agent (H_2O_2/Fe^{2+}) and the modified Fenton agent (H_2O_2/Fe^{3+}) [12] but also utilizes the transition metal ions and their complexes in low oxidation states such as Cu(I), Cr(II) and Ti(III) to react with H_2O_2 to produce $HO^{\bullet}$ radicals, collectively known as Fenton-like agents [13]. The Fenton catalysis method has the outstanding advantage of i) the ability to catalyze with high reaction kinetics based on the generated highly reactive hydroxyl radicals [14,15]; ii) being widely applied to treat various types of organic pollutants [16]; and iii) being environmentally friendly with less toxic by-products [17]. Nevertheless, the Fenton process does have certain drawbacks when it comes to treating organic matter. These include the limited pH range it operates optimally in (pH 3) and the significant volume of iron slurry, which poses challenges for recycling the homogeneous catalyst (Fe^{2+}) [18]. However, when the solution pH is increased, most of the metal oxide nanoparticles will tend to accumulate on the material's surface, reducing the surface area and hindering the reactants' movement, thereby reducing the catalytic performance of OPs [19]. Therefore, recently the studies on heterogeneous Fenton, the nanoparticles will be fixed on different supports to limit their accumulation. Alumina, silica, zeolite, and activated carbon are reported as the most extensively usual catalyst supports [20–23].

Metal-organic frameworks (MOFs) are a distinct spongy matter category with various captivating attributes, including remarkable surface area, porosity, flexible functionality, and adjustable pore structures. Owing to these exceptional qualities, MOFs have garnered significant interest as excellent catalyst support, attracting considerable attention for their immense potential. UiO-66 comprises $[Zr_6O_4(OH)_4]$ clusters with 1,4-benzo dicarboxylic acid linkage rods among the numerous MOFs. This topic has undergone thorough investigation, primarily driven by its remarkable thermal and chemical stability exhibited in aqueous solutions as well as organic solvents [24,25]. There have been many studies on the application of UiO-66 and its-based composites in adsorption [26], photocatalysis [27], gas separation [28], and analytical electrochemistry [29]. To mitigate the generation of solid waste, such as iron precipitates, at low pH conditions, the incorporation of Fe_3O_4 and Cu_2O oxides onto UiO-66 has been employed as a catalyst for Fenton-type reactions. This approach leverages the favourable oxidizing capacity of the catalyst while reducing the likelihood of metal precipitation [30–32]. Therefore, combining these two oxides is more and more meaningful in improving the catalytic ability for the breakdown of organic impurities in aquatic medium.

In this study, we synthesized Cu_2O/Fe_3O_4/UiO-66 composite and investigated its performance as a Fenton-like agent for degrading reactive blue 19 (RB19) in water. Two key assumptions guided our study: 1) the inclusion of Cu_2O in the composite, with its low valence transition metal (Cu(I)), enhances the creation of exceptionally active hydroxyl radicals ($HO^{\bullet}$), which are crucial for pollutant degradation; 2) UiO-66 immobilizes nanoparticles and attracts pollutant molecules, while Fe_3O_4 acts as the primary catalytic agent and facilitates catalyst recovery and reuse. To assess the validity of these assumptions, statistical techniques were employed to judge the catalytic efficiency of the Fenton reaction. Also, the Random forest (RF) and the SHAP (SHapley Additive exPlanations) models were employed to quantify the impact of various experimental factors on the reaction performance. Furthermore, the study inspected the effect of trial conditions, such as pH, catalyst loading, RB19 and H_2O_2 strength, reaction temperature, and catalyst reusability, on the degradation of RB19 to pinpoint the optimum variables.

2. Materials and methods

2.1. Materials

Benzene-1,4-dicarboxylic acid (H_2BDC, $C_6H_4(CO_2H)_2$, 99%), zirconium(IV) chloride ($ZrCl_4$, 98%), reactive blue 19 ($C_{22}H_{16}O_{11}N_2S_3Na_2$, 50%), N,N′-dimethylformamide (DMF, C_3H_7NO, 99%), methanol (CH_3OH, 99%), sodium hydroxide (NaOH, 97%), ethanol (C_2H_5OH, 99%), iron(II) sulfate heptahydrate ($FeSO_4.7H_2O$, 99%), copper(II) sulfate pentahydrate ($CuSO_4.5H_2O$, 98.0%), hydrochloric acid (HCl, 35%), iron(III) chloride hexahydrate ($FeCl_3.6H_2O$, 98%), and hydroperoxide (H_2O_2, 30%) were acquired from Merck's company (Germany). No additional purification was performed on the analytical reagents before use, and all experimental procedures utilized deionized water.

2.2. Synthesis of catalyst

2.2.1. UiO-66

UiO-66 was fabricated via the hydrothermal method following the procedure outlined in a previous study [33]. A transparent solution was received by ultrasonically liquefying 0.317 g of $ZrCl_4$ and 0.226 g of H_2BDC in 30 mL of DMF solvent. This mixture was then moved into a hydrothermal reactor and subjected to thermal treatment at 120 °C for 36 h in an oven. Once it reached ambient temperature, the resulting white powder was isolated from the resolution through centrifugation, rinsed with ethanol, and dried overnight at 60 °C to acquire UiO-66.

2.2.2. Fe_3O_4

Firstly, the mixture, including 2.6 g of $FeCl_3$ and 1.2 g $FeSO_4$ in $NaOH/C_2H_5OH$ solution (5 g/100 mL) was swirled magnetically for 2 h (60 °C) and then conveyed to a heat-resistant Teflon flask and maintained at 90 °C for 6 h. Upon reaching ambient temperature, the solid materials underwent several cycles of rinsing with C_2H_5OH and distilled water. Subsequently, they were dried at 60 °C for 8 h to obtain Fe_3O_4 powder.

2.2.3. Cu_2O nanoparticles

Cu_2O nanoparticles were prepared through a chemical reduction approach utilizing ascorbic acid as the reducing agent. Initially, 10 g of $CuSO_4.5H_2O$ was blended in 400 mL of distilled water. Subsequently, 0.8 g of ascorbic acid and 1.2 g of NaOH were added to the solution. The resulting product was obtained by centrifugation, followed by multiple rinses with water. Finally, it was dried at 60 °C under vacuum conditions in an oven for a day.

2.2.4. Cu_2O/Fe_3O_4/UiO-66

A mixture of 0.24 g Fe_3O_4, 0.24 g Cu_2O, 0.634 g $ZrCl_4$, and 0.452 g H_2BDC was placed into a 100 mL Teflon-lined. A volume of 60 mL DMF was added, and ultrasound was employed to aid in the dissolution of the solids. The autoclaving machine was then warmed over 120 °C and kept for 36 h. Once the temperature has equilibrated to room level, a magnetic field separated the solid material from the solution. It was then cleaned several times (ethanol, DMF) and and subsequently evaporated at 60 °C for 24 h, forming Cu_2O/Fe_3O_4/UiO-66.

2.3. Experimental procedure

We assessed the catalytic degradation of RB19 by Cu_2O/Fe_3O_4/UiO-66 in a 50 mL glass flask equipped by magnetic-induced stirring. The pH level of the RB19 was changed by either 0.1 M NaOH or 0.1 M HCl. An amount of 40 mg of the catalyst was combined with the RB19 solution (25 mL, 100 mg/L) while being stirred continuously for 2 h to attain the sorption equipoise. Subsequently, 1 mL of 4 M H_2O_2 was introduced to initiate the Fenton-catalyzed reaction. The retrieval of the heterogeneous Fenton catalyst from the post-reaction solution is accomplished by employing an external magnetic field, enabling its subsequent reuse. We conducted optimization experiments for the Fenton catalyst under similar conditions, varying the pH from 3 to 9, the amount of catalyst used varied between 0.4 and 2.0 g/L, RB19 strength from 50 to 200 mg/L, H_2O_2 concentrations from 0.08 M to 0.2 M, and thermal condition ranging from 25 to 55 °C.

The concentrations of RB19 at different reaction times were confirmed by the UV–Vis spectroscopy procedure (Cary 60, Agilent, USA) at 595 nm. All experiments were conducted in triple measurements. The efficiency of RB19 degradation by catalysts was evaluated using Eq. (1):

$$\text{Degradation efficiency } (\%) = (C_o - C_t)/C_o \text{ x } 100\% \quad (1)$$

where t (min) represents the reaction time, C_o and C_t (mg/L) indicates the initial level and concentration of RB19 at any given time required for the reaction t, respectively.

Following the reaction, Cu_2O/Fe_3O_4/UiO-66 composite was isolated via filtration, cleansed with water and ethanol, and reclaimed for a fresh response following a 24-h drying period at 60 °C. This sequence of steps was iterated numerous times to assess the reusability of Cu_2O/Fe_3O_4/UiO-66 composite.

2.4. Characterization

The catalysts' structure was characterized using various techniques. An FE-SEM working at an acceleration electrical force of 5.0 kV was employed to provide a detailed description. The crystal structure and phase purities were examined using a powder X-ray diffractometer (XRD) with CuKα radiation ($\lambda = 0.15406$ nm). The material underwent FTIR measurements to depict the existence of functional groups. Further, elemental analysis was conducted operating energy-dispersive X-ray (EDX) spectroscopy. The nitrogen adsorption/desorption isotherm was recorded using a volumetric adsorption analyzer system to determine the catalyst's surface area, and the Brunauer-Emmett-Teller (BET) model evaluated its catalyst. Thermogravimetric analysis (TGA) was realized under atmospheric pressure on a TG-DTA instrument, employing a rate of temperature rise of 10 °C per second, to investigate the catalyst's thermal behavior.

2.5. Statistics and machine learning

The Shapiro-Wilk test is a statistical method used to assess whether a given sample of data follows a normal distribution. It examines the null hypothesis that the data are drawn from a normal distribution. If the calculated p-value is greater than the chosen specific level of 0.05, the null hypothesis will not be rejected. In that case, the data can be assumed to exhibit a normal distribution. The Shapiro-Wilk test is commonly implemented in statistical software such as R using the Shapiro test function.

ANOVA (Analysis of Variance) compares means between two or more groups. The test's purpose is to evaluate the null hypothesis - no significant difference among the means of the segments. If the ANOVA test indicates a significant difference, Tukey's Honest Significant Difference (TukeyHSD) is typically conducted to determine which specific group means differ significantly. TukeyHSD

compares all possible pair-wise differences between group means.

ML refers to a tool or "machine" which "learn" data to output useful things without being explicitly programmed. A typical ML project is gathering a dataset and algorithmically developing a statistical model that can address practical tasks [34]. ML, specifically supervised learning, differs from statistics in that it starts with a collection of input-output pairs rather than assumptions. Supervised learning aims to apply a learning algorithm to the training dataset to map inputs to outputs [35].

Here we used RF algorithm and SHAP method for driver analysis. RF is an ensemble ML algorithm of decision trees, selecting random subsets of features and samples to make predictions [36]. SHAP originated from Shapley values - based on game theory, which assigns a fair distribution of a cooperative gain or loss to each player in a game [37]. In the context of ML, the SHAP method assigns a contribution score to each input feature that reflects its impact on the model's output [38]. These SHAP values were calculated using RF model, which maps the input variables (i.e., experimental conditions) to the output variable (C/C_o). The SHAP method and RF were implemented using Python programming language with packages of "sklearn", "RandomForestRegressor", and "shap" [39].

3. Results and discussion

3.1. Characterization of catalyst

FE-SEM images were utilized to characterize the morphologies of the prepared materials (Fe_3O_4, Cu_2O, UiO-66, and Cu_2O/Fe_3O_4/UiO-66). The UiO-66 particles displayed a hexagonal uniform shape with a size from 100 to 150 nm (Fig. 1a), similar to the public of Maite Perfecto-Irigaray et al. [40]. Fe_3O_4 particles had a spherical shape of 100–300 nm in diameter and agglomerated into clusters (Fig. 1b). Meanwhile, the Cu_2O sample exhibited octahedral morphology with a scale covering between 100 and 200 nm (Fig. 1c). The FE-SEM image of Cu_2O/Fe_3O_4/UiO-66 (Fig. 1d) revealed that the composite consisted of different shapes and sizes. To further identify the successful production of material (Cu_2O/Fe_3O_4/UiO-66), the EDX analysis was used to detect the presence of elements in the prepared material. According to the EDX spectra shown in Fig. 1e, the composite contained the primary elements (C, O, Fe, Cu, and Zr) of the three individual components, indicating the existence of Cu_2O, Fe_3O_4, and UiO-66 phases in the material. The EDX mapping of the as-prepared composite in Fig. 1f indicated the uniform diffusion of primary elements in the same region. The XRD analysis also supports this statement. According to Fig. 2a, the prominent peak at 6^o and 9.7^o shows the presence of UiO-66 in the material [41]; the narration of the presence of Fe_3O_4 corresponds to the characteristic peaks at 30.2^o, 35.8^o, 57.9^o [42] and Cu_2O corresponding to 36.6^o and 42^o [43]. The FTIR of individual components were recorded to verify the surface functional groups, and the result is depicted in Fig. 2b. In the FTIR results of two developed materials (Fe_3O_4/UiO-66 & Cu_2O/Fe_3O_4/UiO-66), the highest point at 550 cm^{-1} matched the vibrational elongation of Fe–*O*–Fe, indicating that Fe_3O_4 is existed in the composite [44]. The peak around 749 cm^{-1} corresponds with the O–Zr–O vibration, and other undersized peaks found from 700 to 1200 cm^{-1} were associated with the oscillations in aromatic rings of UiO-66 material [45]. Moreover, the clear apices at 1395, 1586, and 1654 cm^{-1} can be credited to the occurrence of the UiO-66 carboxyl groups [46,47]. The richness of carboxyl groups will facilitate the immobilization of Fe_3O_4 and Cu_2O nanoparticles on the UiO-66 surface through complexation and electrostatic interactions [4].

The porousness and outer surface of Cu_2O/Fe_3O_4/UiO-66 were evaluated based on the nitrogen adsorption/desorption isotherm (Fig. 3a). Based on the testing results, it was found that the sample exhibited the type IV isotherm along with a hysteresis loop, within the relative pressure interval of 0.7–0.9. Based on these findings, it can be inferred that the catalyst possesses a mesoporous structure [48]. The surface area determined by the BET analysis yielded a value of 35.45 m^2/g. This value is not as high as pure UiO-66 (1044.27

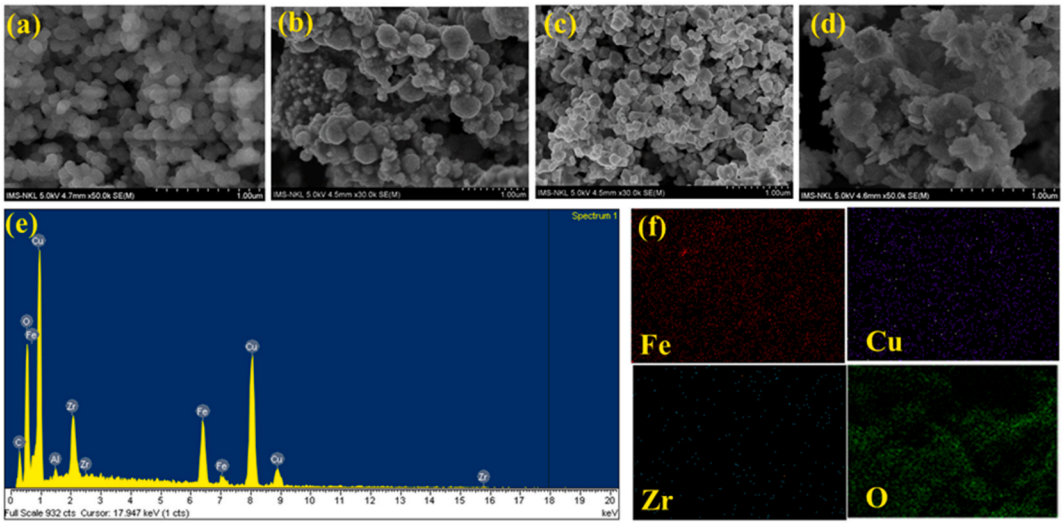

Fig. 1. SEM images of UiO-66 (a), Fe_3O_4 (b), Cu_2O (c) and Cu_2O/Fe_3O_4/UiO-66 (d); EDX spectra (e) and elemental mapping of Cu_2O/Fe_3O_4/UiO-66 (f).

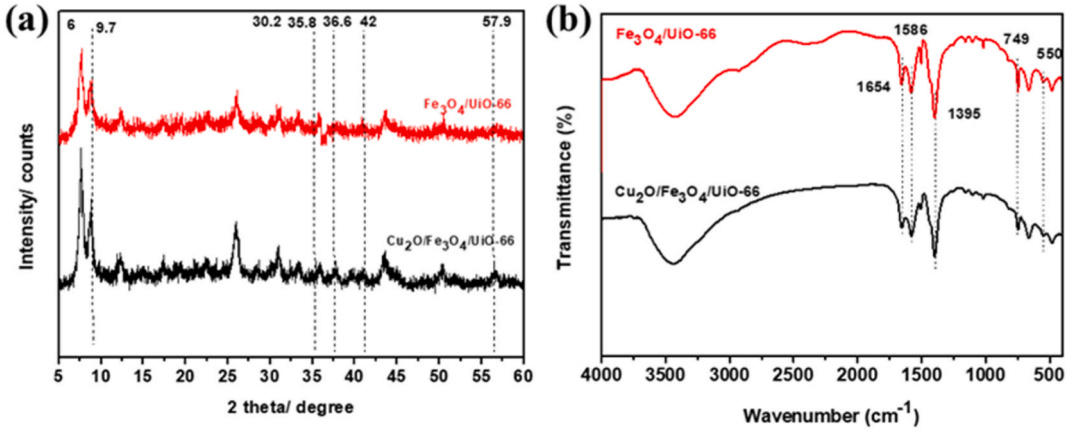

Fig. 2. XRD (a) and FTIR (b) images of Fe_3O_4/UiO-66 and Cu_2O/Fe_3O_4/UiO-66.

m^2/g) [29] because immobilized nanoparticles obscure the surface. The BJH method was further exerted to confirm the distribution of pore sizes within the catalyst. According to the pore size distributions curves depicted in Fig. 3b, the pores of Cu_2O/Fe_3O_4/UiO-66 distributed mainly in the range of 5.5–13.4 nm with the apex at 9.2 nm, which belongs to the range mesoporous [49].

TGA instrument also functioned at the range of 25–800 °C to evaluate the temperature resilience of the prepared Cu_2O/Fe_3O_4/UiO-66 nanocomposite. As presented in Fig. 3c, the first weight loss stage, about 9.95% at temperatures below 150 °C can be credited to the vaporization, moisture absorbed on surfaces, and residual solvents in the material. The second decline of 6.74% in the range of 253.52–434.19 °C can be related to the removal of DMF, which was used in the synthesis and washing of the product. The weight loss of the catalyst was about 36% at 450–600 °C, which aligned to the heat-based breakdown of the framework architecture of UiO-66 because the linker-organic molecules in the structure were combusted [50]. After that, there was no appreciable change in mass as the temperature rose to 800 °C. Thus, the results indicated that Cu_2O/Fe_3O_4/UiO-66 was thermally stable at temperatures below 450 °C.

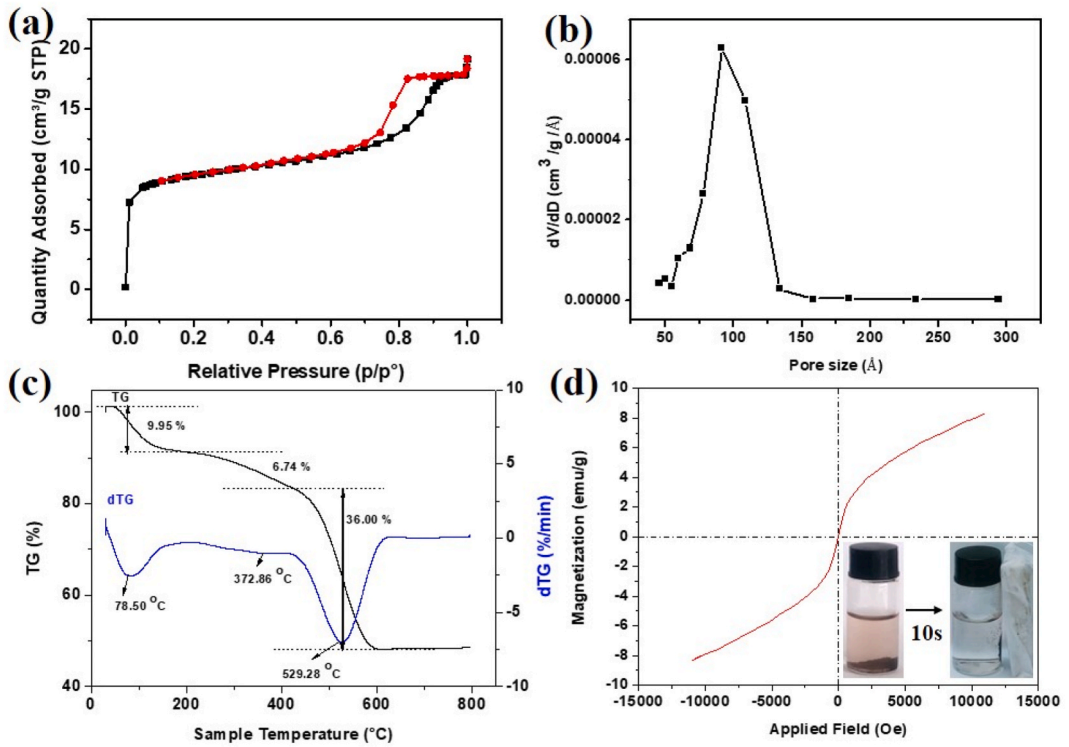

Fig. 3. N_2 adsorption–desorption isotherms (a); pore dimension dispersion (b); TGA isotherm curve (c) and magnetization curve of Cu_2O/Fe_3O_4/UiO-66 (d).

The presence of Fe_3O_4 particles within the composite structure imparts magnetic properties to the material, enabling convenient retrieval of the catalyst using an extrinsic magnetic field. The magnetic behavior of the Cu_2O/Fe_3O_4/UiO-66 sample was investigated using a vibrating sample magnetometer, and the resulting magnetization curve is depicted in Fig. 3d. The value of complete magnetization calculated from the magnetization curve is 8.4 emu/g with a hysteresis loop, indicating that the material has good response strength at different magnetic fields. Although the saturation value of Cu_2O/Fe_3O_4/UiO-66 is smaller than that of some other published ferromagnetic materials (69.69 emu/g of Fe_3O_4 nanoparticle [51], 15.53 emu/g of UiO-66/Fe_3O_4/GO [52]), an external magnet can easily collect the material after dispersing in an aqueous medium for 10 s.

3.2. Fenton-like catalytic activity

The catalytic capability of Cu_2O/Fe_3O_4/UiO-66 composite was investigated by the degradation of RB19 from the Fenton reaction. According to Fig. 4a, the UV–Vis observation indicated the absorption band of RB19 at 595 nm. The intensity of this band decreased with increasing the time reaction and was almost absent later 90 min of the Fenton reaction system. To further research the Fenton reaction-mediated removal of RB19, in the immersing test, the catalyst was filtered out after 30 min of reaction with the existence of H_2O_2 and measured the concentration of RB19 at the time of reaction. Compared to the experiment using the catalyst in 90 min of the reaction (Fig. 4b), the decolorization of RB19 was stopped when separated the catalyst by an external magnet, indicating that Cu_2O/Fe_3O_4/UiO-66 was the heterogeneous catalyst in the Fenton system for breakdown of RB19.

($t_{reaction}$ = 25 °C; C_o = 100 mg/L; dose catalyst = 1.6 g/L, [H_2O_2] = 0.16 M; pH 7).

Various materials (without catalyst, UiO-66, Fe_3O_4, Fe_3O_4/UiO-66, and Cu_2O/Fe_3O_4/UiO-66) were subjected to batch experimentations to estimate and compare their respective degradation efficiencies of RB19. As depicted in Fig. 4c, the concentration of RB19 did not change significantly in the absence of a catalyst, revealing the poor oxidation ability of H_2O_2 with RB19. In contrast, RB19 was rapidly degraded with the presence of the catalysts. For UiO-66, the concentration of RB19 decreased quickly in the initial stage of the reaction, reaching 27% within 15 min, and then remained almost unchanged. This proves that UiO-66 has relatively weak Fenton catalytic activity. Compared to UiO-66 and Fe_3O_4, the degradation efficiency of Fe_3O_4/UiO-66 decreased steadily during the survey period and reached 63% in 90 min, demonstrating that the presence of Fe_3O_4 in the material increased the catalytic performance due to its strong Fenton oxidation capability. Morphology of Fe_3O_4 consists of heavily agglometated particles due to magnetic property in nature. Therfore it used alone shows very poor photocatalytic degradation. However as Fe_3O_4 nanoparticle was highly dispered on the UiO-66 matrix with large surface area the Fe_3O_4/UiO-66 presents the better catalytic activity toward the RB19 degradation. The Cu_2O/Fe_3O_4/UiO-66 possessed the highest catalytic activity with a degradation performance of 83.9% in 90 min thanks to the introduction of Cu_2O. Moreover, the Fenton-like reaction rate constant (k, min^{-1}) was determined from the exponential decay model $\ln(C_t/C_o) = -kt$. The resulting plots of $\ln(C_t/C_o)$ versus t for all samples were linear with coefficients of determination ranging from 0.70 to 0.99, demonstrating that the kinetic model well described the kinetics of the degradation of RB19 (Fig. 4d). The k value of Cu_2O/Fe_3O_4/UiO-66 was calculated to be 0.0196 min^{-1}, which was higher than that of Fe_3O_4/UiO-66 (0.0112 min^{-1}), UiO-66

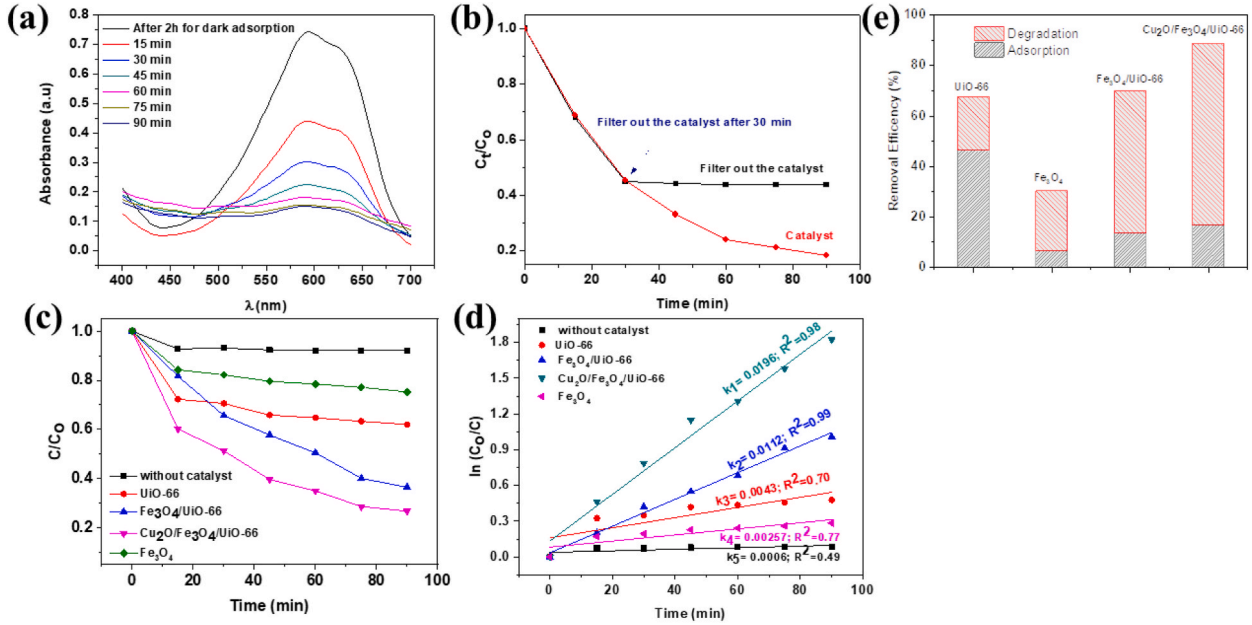

Fig. 4. The UV–Vis spectra of RB19 in 90 min degradation (a); the immersing experiment (b); the Fenton catalytic degradation of RB19 in the presence of UiO-66, Fe_3O_4, Fe_3O_4/UiO-66, Cu_2O/Fe_3O_4/UiO-66, and without the catalyst (c); linear fitting of the catalytic degradation (d); the comparision of RB19 removal efficiency between adsorption and degradation (e).

(0.0043 min^{-1}) and Fe_3O_4 (0.00257 min^{-1}). The above results indicated sufficient evidence for the highly effective Fenton-like capacity of Cu_2O/Fe_3O_4/UiO-66 for RB19 degradation.

The presence of Cu in the material is believed to boost the catalytic reaction rate compared to the rest of the materials. On the one hand, adding Cu_2O in the composite provided more active sites for H_2O_2 decomposition, increasing the generation of reactive oxidants such as $HO^{\bullet}$, thereby enhancing the catalytic capacity [53]. In contradistinction, rising electron density when Fe combines with Cu on the UiO-66, makes the oxidation process more favourable. At the same time, the coordination of Cu and Fe in the Zr–O clusters of UiO-66 can expand the material's pore size, facilitate mass transfer and increase the catalytic efficiency [54,55].

Fig. 4e illustrates the capacity to eliminate RB19 concerning the catalysts' adsorption process, indicating that UiO-66 material exhibits superior catalytic efficiency attributable to its porous structure, expansive surface area, and the presence of functional groups within UiO-66. Compared to Fe_3O_4 and Fe_3O_4/UiO-66, Cu_2O/Fe_3O_4/UiO-66 material obtained a higher ability to remove RB19 for both adsorption and Fenton catalysis thanks to the presence of Cu_2O and Fe_3O_4 on the catalyst surface. Thus, Cu_2O/Fe_3O_4/UiO-66 is considered an appropriate catalyst that can balance the adsorption and decomposition of RB19 in solution in the presence of H_2O_2 with the highest efficiency.

The statistical methods employed in this study aimed to determine whether the catalytic systems, specifically C/C_o of UiO-66, Fe_3O_4/UiO-66, and Cu_2O/Fe_3O_4/UiO-66, had a significant impact on the degradation of reactive dye compared to random variations. The Shapiro test results inferred that the data was a Gaussian bell curve ($p > 0.05$). The findings revealed that all catalysts improved dye degradation compared to the control experiment (i.e., no catalyst), as depicted in Fig. 5. The comparison between UiO-66 and Fe_3O_4/UiO-66 betrayed no considerable discrepancy in the mean C/C_o values ($P > 0.05$, and the Confidence interval (C.I.) at 95% encompassed zero). In contrast, the analysis indicated significant differences in the mean C/C_o values for other groups of catalysts. Specifically, the comparisons involving no catalyst with Cu_2O/Fe_3O_4/UiO-66 and Fe_3O_4/UiO-66, as well as Cu_2O/Fe_3O_4/UiO-66 with Fe_3O_4/UiO-66 and UiO-66, exhibited statistically significant disparities. The target catalyst, Cu_2O/Fe_3O_4/UiO-66, demonstrated a substantial difference in C/C_o compared to the case without any catalyst ($p = 10^{-6}$), with 95% C.I. deviating from zero. The results of the statistical tests strongly support the hypothesis that the developed catalyst, Cu_2O/Fe_3O_4/UiO-66, outperformed the control catalyst in the degradation of the reactive dye.

3.3. Effects of experimental conditions

The trial conditions, including pH, dye concentration, catalyst dosage, temperature, and H_2O_2 concentration, significantly affect dye degradation [22]. Therefore, the degradation of RB19 by Cu_2O/Fe_3O_4/UiO-66 under different experimental conditions was studied. In Fig. 6a, the time-dependent degradation of RB19 is presented, showcasing variations observed at different pH levels. Generally, the removal of RB19 was effective at low pH values, and the best performance was observed at pH 3. This is consistent with the knowledge that the Fenton reaction attains optimum degradation efficiency at a pH value of 3 [56]. Under an acidic environment, the increased removal efficiency of RB19 can be ascribed to the enhanced oxidation potential of $HO^{\bullet}$ radicals and the more leaching of Cu, Zr, and Fe species [57]. The catalyst remained effective at pH 5 and 7 with RB19 removal efficiency of 86.0% and 83.9%, respectively. However, at a pH higher than 7, the degradation of RB19 was notably reduced. Due to the corrosive nature of low pH, which can harm the catalyst, a neutral pH was preferred for this study. Therefore, a pH value of 7 was selected for the subsequent experiments.

The influence of varying catalyst levels on the decomposition of RB19 by Cu_2O/Fe_3O_4/UiO-66 composite is shown in Fig. 6b. It was observed that the degradation rate of RB19 showed a direct correlation with the increasing dose of the catalyst. This can be explained by more reactive sites, promoting H_2O_2 decomposition reactions to generate more free radicals [58]. The RB19 removal efficiency was 35.5% with the loading of 0.4 g/L and up to 83.5% when the dosage level was escalated to 1.6 g/L. However, when the amount of Cu_2O/Fe_3O_4/UiO-66 added was raised to 2 g/L, the removal efficiency of RB19 was not further increased, presumably because of the scavenging of $HO^{\bullet}$ radicals and the aggregation of particles [6]. The most favourable catalyst quantity, as per the findings, was identified as 1.6 g/L.

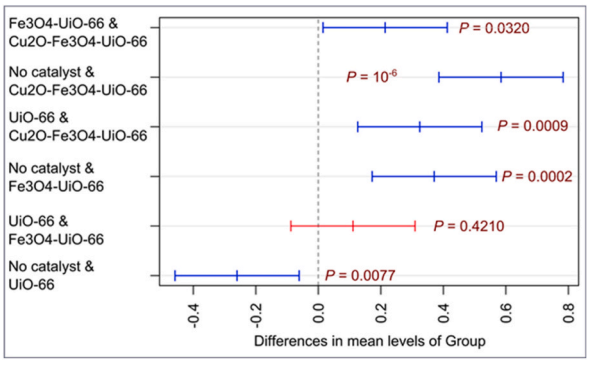

Fig. 5. Results of ANOVA and Tukey HSD test between pair-wise groups (C/C_o of UiO-66, Fe_3O_4/UiO-66, and Cu_2O/Fe_3O_4/UiO-66) at 95% confidence level.

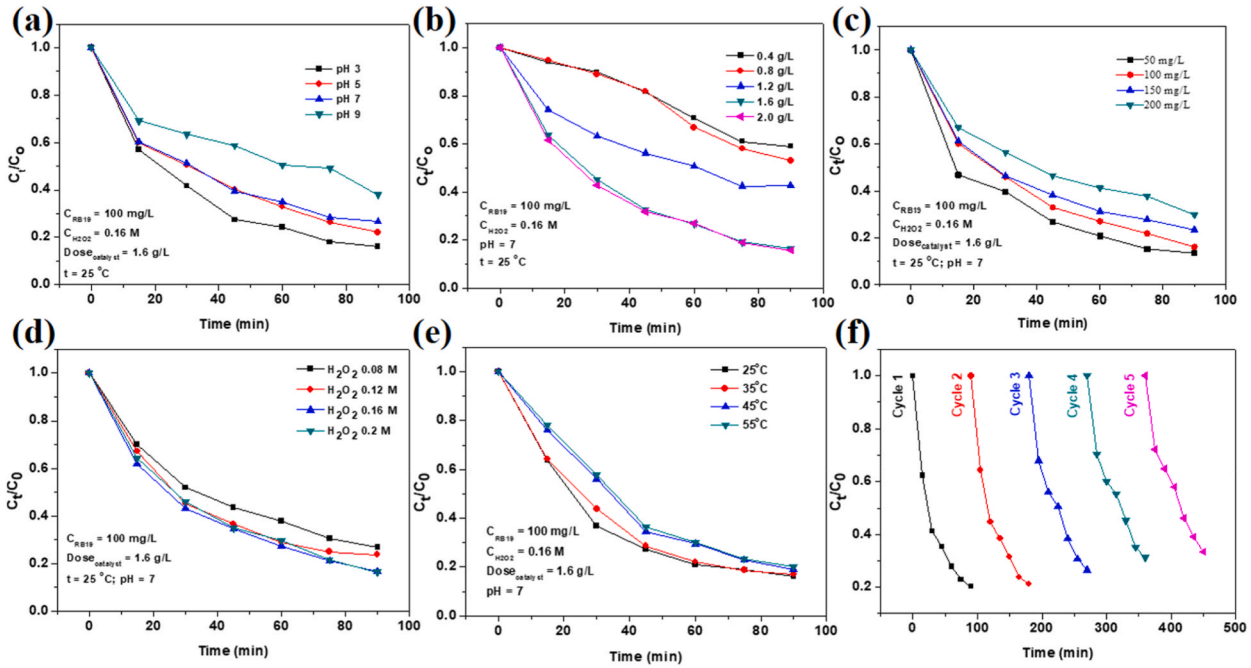

Fig. 6. The effect of pH (a); the dose of catalyst (b); the concentration of RB19 (b); the concentration of H_2O_2 (d); the temperature reaction (e) on RB19 hydroxylation; and the reusability (f) of Cu_2O/Fe_3O_4/UiO-66 after degradation of RB19.

To examine the impact of the original level, the RB19 concentration was altered in the span of 50–200 mg/L. The lower the initial concentration, the faster the degradation of RB19 occurred (Fig. 6c). The removal performance achieved 86.5%, 84.9%, 76.7%, and 71.2% within 90 min of reaction when the initial RB19 concentrations were set at 50, 100, 150, and 200 mg/L, respectively.

The impact of H_2O_2 level was inspected across 0.08–0.2 M (Fig. 6d). The degradation of RB19 depicted a gradual increase as the H_2O_2 strength rose from 0.08 to 0.16 M. The phenomenon can be explained by the increased generation of reactive oxidation groups, specifically hydroxyl radicals, resulting from higher exposure of the catalyst to H_2O_2.When the concentration of H_2O_2 increased from 0.16 to 0.2 M, the breakdown of RB19 did not change much (83.4% for H_2O_2 0.16 M and 0.2 M) because the perhydroxyl radicals $^{\bullet}OHH$ generated from H_2O_2 were paired with the hydroxyl radicals (Eqs. (2) and (3)), reducing the reactive radicals [56].

$$H_2O_2 + {}^{\cdot}OH \rightarrow H_2O + {}^{\cdot}OHH \quad (2)$$

$$^{\cdot}OHH + {}^{\cdot}OH \rightarrow H_2O + O_2 \quad (3)$$

The impact of varying reaction thermal conditions between 25 and 55 °C on the degradation of RB19 using Cu_2O/Fe_3O4/UiO-66 was investigated. According to Fig. 6e, with the rising reaction temperature from 25 to 55 °C, the catalytic capacity gradually decreased from 83.9 to 79.8% due to the heat-related decomposition mechanism of H_2O_2 to O_2 and H_2O at intense thermal conditions [59]. Therefore, the suitable temperature for the Fenton degradation of RB19 was selected as 25 °C.

3.4. *Reusability of Cu_2O/Fe_3O_4/UiO-66*

The study on the reusability of the Cu_2O/Fe_3O_4/UiO-66 catalyst was carried out in five consecutive cycle reactions. The condition

Table 1
The comparison of catalytic effectivity with the reaction conditions of catalysts.

Catalyst	Photocatalytic/Fenton	K (min^{-1})	C_o(mg/L)/dose of catalyst (g/L)/pH	Refs.
α-Fe_2O_3/WO3	Photocatalytic	–	10/1/2	[61]
AgBr/$BiPO_4$/g-C_3N_4	Photocatalytic	0.0785	20/1/3	[62]
g-C_3N_4	Photocatalytic	0.0096	20/1/3	[62]
$BiPO_4$/g-C_3N_4	Photocatalytic	0.0159	20/1/3	[62]
La^{3+}/S/TiO_2	Photocatalytic	–	25/1/-	[63]
$Mg_{0.5}Ni_{0.4}Zn_{0.1}Fe_2O_4$	Photocatalytic	0.0734	25/0.3/5	[64]
$Mg_{0.5}Zn_{0.5}Fe_2O_4$	Photocatalytic	0.0243	25/0.3/5	[64]
Bentonite clay modified with Nb_2O_5	Photocatalytic with the presence of H_2O_2	–	30/0.5/3	[65]
ZnO nanoparticle	Photocatalytic	–	10/0.21/-	[66]
Cu_2O/Fe_3O_4/UiO-66	Fenton	0.0196	100/1.6/7	This study

reactions were set up as follows: loading of catalyst of 1.6 g/L, dye strength of 100 mg/L, pH of 7, H_2O_2 concentration of 0.16 M, and reaction temperature of 25 °C. Following each cycle, the catalyst underwent a washing step with distilled water, subsequent drying, and was then employed for the subsequent reaction. The efficacy of the removal process of RB19 dropped moderately with increasing the number of recycles (Fig. 6f). The degradation performance after five recycles reduced by about 13% compared to the first use. The decrease in the catalytic activity of Cu_2O/Fe_3O_4/UiO-66 can be attributed to the drop of the agent during washing and the hardening of the reaction sites due to the binding of the intermediates [60]. However, after five consecutive runs, the prepared material maintained a high catalytic activity (70%). The results indicated that Cu_2O/Fe_3O_4/UiO-66 has good reusability and stability and can be used for a long time.

Table 1 compares different catalysts' RB19 removal catalytic capacities with the respective reaction conditions. As seen in Table 1, the Cu_2O/Fe_3O_4/UiO-66 catalyst has a relatively good removal of RB19 at neutral pH (pH 7) with a high concentration of RB19. While the remaining catalysts mainly perform at low pH. This is an advantage of the material that can perform RB19 removal in a friendly and less toxic environment.

3.5. Influencing factors

The consequence of different reaction variables, such as reaction time, pH value, reaction temperature, H_2O_2, and RB19 strengths, on the catalytic performance of RB19 through the Fenton reaction was examined. The SHAP values were utilized to determine the relative importance of these experimental factors in influencing the C/C_o results. This consequence of data driven-ML model supports to explain the catalyst behavior and degradation processes based on data.

A distinct color characterizes each parameter value, and the resulting SHAP value on the x-axis shows the contribution of the raw component. The reaction time and pH value were the highest-ranking features, continued by the concentration of H_2O_2, temperature reaction and initial concentration of RB19 (Fig. 7). In a study on the mechanism for enhancing heterogeneous Fenton reaction kinetics, Zhang et al. (2020) demonstrated that the reaction time significantly influences Fenton performance [67]. Longer reaction times generate more hydroxyl radicals, increasing catalytic efficiency. However, prolonged times can result in hydroxyl radical degradation through self-reactions or reactions with intermediates [56]. Additionally, extended reaction times may cause iron oxide precipitation, further reducing catalytic efficiency. Therefore, significant attention is devoted to determining the optimal reaction time for specific catalytic reactions aimed at degrading organic pollutants. The pH value significantly impacted the catalytic performance within the Fenton system following the reaction time. An elevated pH can reduce catalytic efficiency, likely due to the superior effectiveness of the reaction catalyst's active sites under acidic conditions [68]. Modifications in pH can influence proton availability, as well as protonation or deprotonation steps, thereby affecting the rate of the reaction.

Consequently, optimizing the pH value becomes crucial as it strongly influences the catalytic efficiency within the Fenton system. Compared with the time reaction and pH value, the impact of the remaining factors such as concentration of H_2O_2, temperature reaction and initial concentration of RB19 did not significantly affect the catalytic performance. Utilizing SHAP, the model elucidated diverse reaction parameters' impact on the Fenton system's catalytic efficiency. This valuable insight aids researchers in comprehending influential factors and refining these parameters, enabling the community to optimize reaction conditions. By adjusting reactant concentration, catalyst type and concentration, pH level, temperature, and reaction time, the community can enhance the efficiency, selectivity, and overall performance of the Fenton reaction across diverse applications.

3.6. Mechanism for Fenton-like reaction

The RB19 breakdown by the Cu_2O/Fe_3O_4/UiO-66 composite follows a proposed reaction mechanism that depends on the electron transfer happening at the active centers of Cu–Fe–Zr on the material (Fig. 8). The presence of Fe was the primary reagent for the production of $HO^{\bullet}$ radical when Fe(II) reacts with H_2O_2.

In the beginning, H_2O_2 adheres to the catalyst's external surface and interacts with Fe(III) within the Fe_3O_4 framework, resulting in

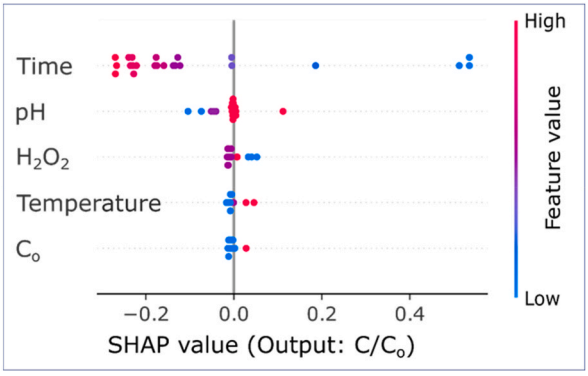

Fig. 7. SHAP plot indicates the impact of raw ingredients on catalytic performance.

the formation of Fe(II), $HO_2^{\bullet}$ and H^+ ions, as dispicted in Eq. (4) and Eq. (5). Consequently, Fe(II) further engages with H_2O_2, leading to the generation of hydroxyl radicals $OH^{\bullet}$ (Eq. (6) and Eq. (7)). The presence of Cu in the structural material can contribute to the enhancement of the generation of free radicals [4,53,55].

$$(Fe^{III}\text{–OH}) + H_2O_2 \rightarrow (Fe^{III}\text{–OH}).(H_2O_2) \quad (4)$$

$$(Fe^{III}\text{–OH}).(H_2O_2)\text{–OH} \rightarrow Fe^{II} + HO_2^{\bullet} + H_2O \quad (5)$$

$$Fe^{II} + H_2O_2 \rightarrow Fe^{III}\text{–OH} + OH^{\bullet} \quad (6)$$

$$Fe^{III}\text{–OH} + HO_2^{\bullet} \rightarrow Fe^{II} + H_2O + O_2 \quad (7)$$

$$Fe^{III} + Cu^{I} \rightarrow Cu^{II} + Fe^{II} \quad (8)$$

$$Cu^{I} + H_2O_2 \rightarrow Cu^{II}\text{–OH} + OH^{\bullet} \quad (9)$$

$$Cu^{II}\text{–OH} + H_2O_2 \rightarrow (Cu^{II}.\ H_2O_2)\text{–OH} \quad (10)$$

$$(Cu^{II}.\ H_2O_2)\text{–OH} \rightarrow Cu^{I} + HO_2^{\bullet} + H_2O_2 \quad (11)$$

$$Cu^{II}\text{–OH} + HO_2^{\bullet} \rightarrow Cu^{I} + H_2O + O_2 \quad (12)$$

So, Cu_2O/Fe_3O_4/UiO-66 was a reservoir for Fe and Cu to release Fe(II) ions to trigger the cleavage of H_2O_2 molecules into $OH^{\bullet}$ radicals (Eq. (8) and Eq. (9)). Alternatively, the Zr centre within the UiO-66 structure plays a crucial role as an electric charge bridge, facilitating electron transfer in a Fenton-like reaction system. It can receive electrons from $O_2^{\bullet-}$, thereby promoting the generation of O_2 [69]. Upon combining Fe_3O_4 nanoparticles with UiO-66, Fe(II) and Zr interactions can occur through the formation of Fe(II)–*O*–Zr(IV) bonds. These interactions make it easier for Fe_3O_4 to lose electrons, thus enhancing the reduction of H_2O_2 and generating $OH^{\bullet}$ radicals [70,71]. The catalyst's Zr centre, characterized by its high charge density, contributes to the interaction between Fe and Cu. This interaction facilitates substantial electron transfer between the Cu–Fe–Zr active centers on the catalyst, leading to increased production of free radicals (Eq. (10) – Eq. (12)) [69]. When the catalyst decomposition occurs, $HO_2^{\bullet}$ and $OH^{\bullet}$ attack RB19 to form inorganic molecules such as H_2O, CO_2, and less toxic intermediates [72], as described in Eq. (13) and Eq. (14).

$$HO_2^{\bullet} \rightarrow H^+ + O_2^{\bullet-} \quad (13)$$

$$RB19 + OH^{\bullet} \rightarrow CO_2 + H_2O + \text{intermediate} \quad (14)$$

4. Conclusion

The research focuses on developing Cu_2O/Fe_3O_4/UiO-66 materials as heterogeneous Fenton catalysts to break down RB19 in a watery solution in the presence of H_2O_2. The results show that Cu_2O/Fe_3O_4/UiO-66 exhibits higher catalytic efficiency and reaction rate than UiO-66 and Fe_3O_4/UiO-66 for 90 min using reaction conditions (pH 7, reaction temperature 25 °C, H_2O_2 concentration 0.16 M, catalyst dosage 1.6 g/L). ANOVA results demonstrated that Cu_2O/Fe_3O_4/UiO-66 obtained exceptional catalytic properties compared with other materials ($p = 10^{-6}$). The experimental conditions leading to the best performance were pH 7, agent loading of 1.6 g/L, H_2O_2 concentration of 0.16 M, and a reaction temperature of 25 °C. The developed composite prepared in this study is stable and reusable for up to five cycles. SHAP identified reaction time and pH as the most influential factors affecting catalytic efficiency. The system operates under environmentally friendly conditions with a neutral pH, making it suitable for degrading organic pollutants.

Data availability statement

Data will be made available on request.

CRediT authorship contribution statement

Thi Thanh Nhi Le: Writing – review & editing, Writing – original draft, Validation, Methodology, Investigation, Formal analysis, Data curation, Conceptualization. **Hai Bang Truong:** Writing – review & editing, Writing – original draft, Resources, Methodology, Investigation, Formal analysis, Data curation. **Thi Hoa Le:** Writing – original draft, Methodology, Investigation, Formal analysis, Data curation, Conceptualization. **Hoang Sinh Le:** Visualization, Validation, Methodology, Investigation, Data curation. **Thanh Tam Toan Tran:** Resources, Methodology, Investigation, Formal analysis, Data curation. **Tran Duc Manh:** Resources, Methodology, Investigation, Formal analysis, Data curation. **Van Thuan Le:** Software, Resources, Methodology, Investigation, Data curation. **Quang Khieu Dinh:** Writing – review & editing, Writing – original draft, Validation, Supervision, Resources, Methodology, Data curation, Conceptualization. **Xuan Cuong Nguyen:** Writing – review & editing, Writing – original draft, Supervision, Software, Project administration, Formal analysis, Data curation, Conceptualization.

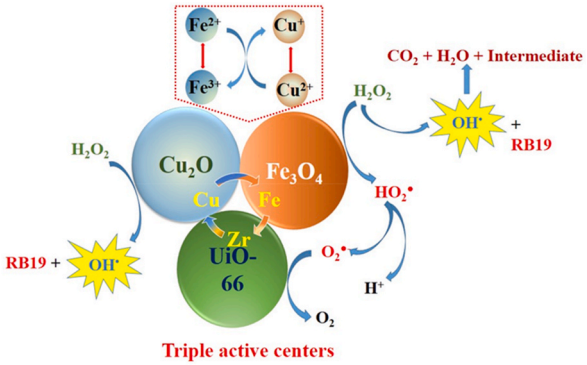

Fig. 8. The suggested degradation mechanism pathway of RB19 employing the Cu_2O/Fe_3O_4/UiO-66 catalyst in Fenton –like reaction.

Declaration of competing interest

The authors declare that they have no known competing financial interests or personal relationships that could have appeared to influence the work reported in this paper.

Acknowledgment

The authors express their gratitude to all the valuable support from Duy Tan University, who is going to celebrate its 30th anniversary of establishment (Nov. 11, 1994–Nov. 11, 2024) towards "Integral, Sustainable and Stable Development".

References

[1] V.-D. Doan, N.-V. Nguyen, T.L.-H. Nguyen, V.A. Tran, V.T. Le, High-efficient reduction of methylene blue and 4-nitrophenol by silver nanoparticles embedded in magnetic graphene oxide, Environ. Sci. Pollut. Res. 30 (2021) 71543–71553, https://doi.org/10.1007/s11356-021-13597-z.
[2] T.H.A. Nguyen, V.T. Le, V.-D. Doan, A.V. Tran, V.C. Nguyen, A.-T. Nguyen, Y. Vasseghian, Green synthesis of Nb-doped ZnO nanocomposite for photocatalytic degradation of tetracycline antibiotic under visible light, Mater. Lett. 308 (2022), 131129, https://doi.org/10.1016/j.matlet.2021.131129.
[3] V.T. Le, V.D. Doan, T.T.N. Le, M.U. Dao, T.T.T. Vo, H.H. Do, D.Q. Viet, V.A. Tran, Efficient photocatalytic degradation of crystal violet under natural sunlight using Fe3O4/ZnO nanoparticles embedded carboxylate-rich carbon, Mater. Lett. 283 (2021), 128749, https://doi.org/10.1016/j.matlet.2020.128749.
[4] V.T. Le, V.D. Doan, V.A. Tran, H.S. Le, D.L. Tran, T.M. Pham, T.H. Tran, H.T. Nguyen, Cu/Fe3O4@carboxylate-rich carbon composite: one-pot synthesis, characterization, adsorption and photo-Fenton catalytic activities, Mater. Res. Bull. 129 (2020), 110913, https://doi.org/10.1016/j.materresbull.2020.110913.
[5] Y. Vasseghian, F. Almomani, V.T. Le, M. Moradi, E.N. Dragoi, Decontamination of toxic Malathion pesticide in aqueous solutions by Fenton-based processes: degradation pathway, toxicity assessment and health risk assessment, J. Hazard Mater. 423 (2022), 127016, https://doi.org/10.1016/j.jhazmat.2021.127016.
[6] V.D. Doan, B.A. Huynh, H.A. Le Pham, Y. Vasseghian, V.T. Le, Cu2O/Fe3O4/MIL-101(Fe) nanocomposite as a highly efficient and recyclable visible-light-driven catalyst for degradation of ciprofloxacin, Environ. Res. 201 (2021), 111593, https://doi.org/10.1016/j.envres.2021.111593.
[7] V.T. Le, V.A. Tran, D.L. Tran, T.L.H. Nguyen, V.-D. Doan, Fabrication of Fe3O4/CuO@C composite from MOF-based materials as an efficient and magnetically separable photocatalyst for degradation of ciprofloxacin antibiotic, Chemosphere 270 (2021), 129417, https://doi.org/10.1016/j.chemosphere.2020.129417.
[8] M.U. Dao, H.S. Le, H.Y. Hoang, V.A. Tran, V.D. Doan, T.T.N. Le, A. Sirotkin, V.T. Le, Natural core-shell structure activated carbon beads derived from Litsea glutinosa seeds for removal of methylene blue: facile preparation, characterization, and adsorption properties, Environ. Res. 198 (2021), 110481, https://doi.org/10.1016/j.envres.2020.110481.
[9] V.D. Doan, V.T. Le, T.T.N. Le, H.T. Nguyen, Nanosized zincated hydroxyapatite as a promising heterogeneous photo-fenton-like catalyst for methylene blue degradation, Adv. Mater. Sci. Eng. 2019 (2019) 1–9, https://doi.org/10.1155/2019/5978149.
[10] C.L. Hsueh, Y.H. Huang, C.C. Wang, C.Y. Chen, Degradation of azo dyes using low iron concentration of Fenton and Fenton-like system, Chemosphere 58 (2005) 1409–1414, https://doi.org/10.1016/j.chemosphere.2004.09.091.
[11] J.C. García, A.M. Pedroza, C.E. Daza, Magnetic Fenton and photo-fenton-like catalysts supported on carbon nanotubes for wastewater treatment, water, Air. Soil Pollut. 228 (2017), https://doi.org/10.1007/s11270-017-3420-7.
[12] S. Wang, A Comparative study of Fenton and Fenton-like reaction kinetics in decolourisation of wastewater, Dye. Pigment. 76 (2008) 714–720, https://doi.org/10.1016/j.dyepig.2007.01.012.
[13] X. Liang, Z. He, Y. Zhong, W. Tan, H. He, P. Yuan, J. Zhu, J. Zhang, The effect of transition metal substitution on the catalytic activity of magnetite in heterogeneous Fenton reaction: in interfacial view, Colloids Surfaces A Physicochem. Eng. Asp. 435 (2013) 28–35, https://doi.org/10.1016/j.colsurfa.2012.12.038.
[14] Y. Hua, S. Wang, J. Xiao, C. Cui, C. Wang, Preparation and characterization of Fe3O4/gallic acid/graphene oxide magnetic nanocomposites as highly efficient Fenton catalysts, RSC Adv. 7 (2017) 28979–28986, https://doi.org/10.1039/c6ra23939k.
[15] K. Barbusiński, Fenton reaction - controversy concerning the chemistry, Ecol. Chem. Eng. S. 16 (2009) 347–358.
[16] Herrmann, Water Treatment by Heterogeneous, Water, 2005, pp. 171–194.
[17] F. Duarte, F.J. Maldonado-Hódar, L.M. Madeira, Influence of the characteristics of carbon materials on their behaviour as heterogeneous Fenton catalysts for the elimination of the azo dye Orange II from aqueous solutions, Appl. Catal. B Environ. 103 (2011) 109–115, https://doi.org/10.1016/j.apcatb.2011.01.016.
[18] S. Yuan, N. Gou, A.N. Alshawabkeh, A.Z. Gu, Efficient degradation of contaminants of emerging concerns by a new electro-Fenton process with Ti/MMO cathode, Chemosphere 93 (2013) 2796–2804, https://doi.org/10.1016/j.chemosphere.2013.09.051.
[19] S.H. Chang, S.H. Chuang, H.C. Li, H.H. Liang, L.C. Huang, Comparative study on the degradation of I.C. Remazol Brilliant Blue R and I.C. Acid Black 1 by Fenton oxidation and Fe0/air process and toxicity evaluation, J. Hazard Mater. 166 (2009) 1279–1288, https://doi.org/10.1016/j.jhazmat.2008.12.042.
[20] O.B. Ayodele, B.H. Hameed, Development of kaolinite supported ferric oxalate heterogeneous catalyst for degradation of 4-nitrophenol in photo-Fenton process, Appl. Clay Sci. (2013) 83–84, https://doi.org/10.1016/j.clay.2013.08.019, 171–181.
[21] J. Herney-Ramirez, M.A. Vicente, L.M. Madeira, Heterogeneous photo-Fenton oxidation with pillared clay-based catalysts for wastewater treatment: a review, Appl. Catal. B Environ. 98 (2010) 10–26, https://doi.org/10.1016/j.apcatb.2010.05.004.

[22] S. Rahim Pouran, A.R. Abdul Aziz, W.M.A. Wan Daud, Review on the main advances in photo-Fenton oxidation system for recalcitrant wastewaters, J. Ind. Eng. Chem. 21 (2015) 53–69, https://doi.org/10.1016/j.jiec.2014.05.005.

[23] A.N. Soon, B.H. Hameed, Heterogeneous catalytic treatment of synthetic dyes in aqueous media using Fenton and photo-assisted Fenton process, Desalination 269 (2011) 1–16, https://doi.org/10.1016/j.desal.2010.11.002.

[24] A.E. Platero-Prats, A. Mavrandonakis, L.C. Gallington, Y. Liu, J.T. Hupp, O.K. Farha, C.J. Cramer, K.W. Chapman, Structural transitions of the metal-oxide nodes within metal-organic frameworks: on the local structures of NU-1000 and UiO-66, J. Am. Chem. Soc. 138 (2016) 4178–4185, https://doi.org/10.1021/jacs.6b00069.

[25] F. Zhang, S. Zheng, Q. Xiao, Y. Zhong, W. Zhu, A. Lin, M. Samy El-Shall, Synergetic catalysis of palladium nanoparticles encaged within amine-functionalized UiO-66 in the hydrodeoxygenation of vanillin in water, Green Chem. 18 (2016) 2900–2908, https://doi.org/10.1039/c5gc02615f.

[26] M. Daraee, E. Ghasemy, A. Rashidi, Synthesis of novel and engineered UiO-66/graphene oxide nanocomposite with enhanced H2S adsorption capacity, J. Environ. Chem. Eng. 8 (2020), 104351, https://doi.org/10.1016/j.jece.2020.104351.

[27] X. Peng, L. Ye, Y. Ding, L. Yi, C. Zhang, Z. Wen, Nanohybrid photocatalysts with ZnIn2S4 nanosheets encapsulated UiO-66 octahedral nanoparticles for visible-light-driven hydrogen generation, Appl. Catal. B Environ. 260 (2020), 118152, https://doi.org/10.1016/j.apcatb.2019.118152.

[28] C.Y. Chuah, J. Lee, J. Song, T.H. Bae, Co2/n2 separation properties of polyimide-based mixed-matrix membranes comprising UiO-66 with various functionalities, Membranes 10 (2020) 1–18, https://doi.org/10.3390/membranes10070154.

[29] L.T.T. Nhi, N.T.T. Tu, L.T. Hoa, T.T.T. Toan, L. Van Thanh Son, N. Van Hung, T.N. Tuyen, D.Q. Khieu, Simultaneous voltammetric determination of ascorbic acid and acetaminophen in pharmaceutical formulations with UiO-66-modified glassy carbon electrode, J. Nanoparticle Res. 23 (2021), https://doi.org/10.1007/s11051-021-05327-w.

[30] B. Sun, H. Li, X. Li, X. Liu, C. Zhang, H. Xu, X.S. Zhao, Degradation of organic dyes over fenton-like Cu2O-Cu/C catalysts, Ind. Eng. Chem. Res. 57 (2018) 14011–14021, https://doi.org/10.1021/acs.iecr.8b02697.

[31] A.J. Luna, C.A.O. Nascimento, O. Chiavone-Filho, Photodecomposition of hydrogen peroxide in highly saline aqueous medium, Braz. J. Chem. Eng. 23 (2006) 341–349, https://doi.org/10.1590/S0104-66322006000300007.

[32] L. Lyu, L. Zhang, C. Hu, Enhanced Fenton-like degradation of pharmaceuticals over framework copper species in copper-doped mesoporous silica microspheres, Chem. Eng. J. 274 (2015) 298–306, https://doi.org/10.1016/j.cej.2015.03.137.

[33] X. Zhang, Y. Yang, L. Song, J. Chen, Y. Yang, Y. Wang, Enhanced adsorption performance of gaseous toluene on defective UiO-66 metal organic framework: equilibrium and kinetic studies, J. Hazard Mater. 365 (2019) 597–605, https://doi.org/10.1016/j.jhazmat.2018.11.049.

[34] V.K. Vemuri, The hundred-page machine learning book, J. Inf. Technol. Case Appl. Res. 22 (2020) 136–138, https://doi.org/10.1080/15228053.2020.1766224.

[35] S.J.R, P. Norvig, Artificial Intelligence: A Modern Approach, Third Edit, 2003.

[36] L. Breiman, Random forests, Mach. Learn. 45 (2001) 5–32, https://doi.org/10.1109/ICCECE51280.2021.9342376.

[37] K.J. Arrow, E.W. Barankin, D. Blackwell, R. Bott, N. Dalkey, M. Dresher, D. Gale, D.B. Gillies, I. Glicksberg, O. Gross, S. Karlin, H.W. Kuhn, J.P. Mayberry, J. W. Milnor, T.S. Motzkin, J. Von Neumann, H. Raiffa, L.S. Shapley, M. Shiffman, F.M. Stewart, G.L. Thompson, R.M. Thrall, Contributions to the Theory of Games, (AM-28), Volume, II, Princeton University Press, 1953.

[38] S.M. Lundberg, S.I. Lee, A unified approach to interpreting model predictions, Adv. Neural Inf. Process. Syst. 2017-Decem (2017) 4766–4775.

[39] D. Pedregosa, G. Varoquaux, A. Gramfort, V. Michel, B. Thirion, O. Grisel, M. Blondel, P. Prettenhofer, R. Weiss, Scikit-learn: machine learning in Python fabian, J. OfMachine Learn. Res. 12 (2011) 2825–2830, https://doi.org/10.1289/EHP4713.

[40] M. Perfecto-Irigaray, G. Beobide, O. Castillo, I. Da Silva, D. García-Lojo, A. Luque, A. Mendia, S. Pérez-Yáñez, [Zr6O4(OH)4(benzene-1,4-dicarboxylato)6]n: a hexagonal polymorph of UiO-66, Chem. Commun. 55 (2019) 5954–5957, https://doi.org/10.1039/c9cc00802k.

[41] Z. Sha, J. Wu, Enhanced visible-light photocatalytic performance of BiOBr/UiO-66(Zr) composite for dye degradation with the assistance of UiO-66, RSC Adv. 5 (2015) 39592–39600, https://doi.org/10.1039/c5ra04869a.

[42] G. Lujanienė, S. Šemčuk, A. Lečinskytė, I. Kulakauskaitė, K. Mažeika, D. Valiulis, V. Pakštas, M. Skapas, S. Tumėnas, Magnetic graphene oxide based nano-composites for removal of radionuclides and metals from contaminated solutions, J. Environ. Radioact. 166 (2017) 166–174, https://doi.org/10.1016/j.jenvrad.2016.02.014.

[43] F. Chai, K. Li, C. Song, X. Guo, Synthesis of magnetic porous Fe3O4/C/Cu2O composite as an excellent photo-Fenton catalyst under neutral condition, J. Colloid Interface Sci. 475 (2016) 119–125, https://doi.org/10.1016/j.jcis.2016.04.047.

[44] X. Sun, G. Gao, D. Yan, C. Feng, Synthesis and electrochemical properties of Fe 3 O 4 @MOF core-shell microspheres as an anode for lithium ion battery application, Appl. Surf. Sci. 405 (2017) 52–59, https://doi.org/10.1016/j.apsusc.2017.01.247.

[45] J.B. Huo, L. Xu, X. Chen, Y. Zhang, J.C.E. Yang, B. Yuan, M.L. Fu, Direct epitaxial synthesis of magnetic Fe 3 O 4 @UiO-66 composite for efficient removal of arsenate from water, Microporous Mesoporous Mater. 276 (2019) 68–75, https://doi.org/10.1016/j.micromeso.2018.09.017.

[46] P. Yang, Q. Liu, J. Liu, H. Zhang, Z. Li, R. Li, L. Liu, J. Wang, Interfacial growth of a metal-organic framework (UiO-66) on functionalized graphene oxide (GO) as a suitable seawater adsorbent for extraction of uranium(VI), J. Mater. Chem. A. 5 (2017) 17933–17942, https://doi.org/10.1039/c6ta10022h.

[47] F. Ahmadijokani, S. Ahmadipouya, H. Molavi, M. Rezakazemi, T.M. Aminabhavi, M. Arjmand, Impact of scale, activation solvents, and aged conditions on gas adsorption properties of UiO-66, J. Environ. Manag. 274 (2020), 111155, https://doi.org/10.1016/j.jenvman.2020.111155.

[48] M. Thommes, K. Kaneko, A.V. Neimark, J.P. Olivier, F. Rodriguez-Reinoso, J. Rouquerol, K.S.W. Sing, Physisorption of gases, with special reference to the evaluation of surface area and pore size distribution (IUPAC Technical Report), Pure Appl. Chem. 87 (2015) 1051–1069, https://doi.org/10.1515/pac-2014-1117.

[49] F.J. Sotomayor, K.A. Cychosz, M. Thommes, Characterization of micro/mesoporous materials by physisorption: concepts and case studies, Acc. Mater. Surf. Res. 3 (2018) 34–50.

[50] S. Kumaraguru, J. Yesuraj, S. Mohan, Reduced graphene oxide-wrapped micro-rod like Ni/Co organic-inorganic hybrid nanocomposite as an electrode material for high-performance supercapacitor, Compos. Part B Eng. 185 (2020), 107767, https://doi.org/10.1016/j.compositesb.2020.107767.

[51] H.X. Zhao, Q. Zou, S.K. Sun, C. Yu, X. Zhang, R.J. Li, Y.Y. Fu, Theranostic metal-organic framework core-shell composites for magnetic resonance imaging and drug delivery, Chem. Sci. 7 (2016) 5294–5301, https://doi.org/10.1039/c6sc01359g.

[52] S. Feng, Z. Ni, S. Feng, Z. Zhang, S. Liu, R. Wang, J. Hu, One-step synthesis of magnetic composite UiO-66/Fe 3 O 4/GO for the removal of radioactive cesium ions, J. Radioanal. Nucl. Chem. 319 (2019) 737–748, https://doi.org/10.1007/s10967-018-6379-y.

[53] M. Faheem, X. Jiang, L. Wang, J. Shen, Synthesis of Cu2O-CuFe2O4 microparticles from Fenton sludge and its application in the Fenton process: the key role of Cu2O in the catalytic degradation of phenol, RSC Adv. 8 (2018) 5740–5748, https://doi.org/10.1039/c7ra13608k.

[54] Z. Zhong, M. Li, J. Fu, Y. Wang, Y. Muhammad, S. Li, J. Wang, Z. Zhao, Z. Zhao, Construction of Cu-bridged Cu2O/MIL(Fe/Cu) catalyst with enhanced interfacial contact for the synergistic photo-Fenton degradation of thiacloprid, Chem. Eng. J. 395 (2020), 125184, https://doi.org/10.1016/j.cej.2020.125184.

[55] T.B. Nguyen, C. Di Dong, C.P. Huang, C.W. Chen, S.L. Hsieh, S. Hsieh, Fe-Cu bimetallic catalyst for the degradation of hazardous organic chemicals exemplified by methylene blue in Fenton-like reaction, J. Environ. Chem. Eng. 8 (2020), 104139, https://doi.org/10.1016/j.jece.2020.104139.

[56] X. Zhang, M. He, J.H. Liu, R. Liao, L. Zhao, J. Xie, R. Wang, S.T. Yang, H. Wang, Y. Liu, Fe3O4@C nanoparticles as high-performance Fenton-like catalyst for dye decoloration, Chin. Sci. Bull. 59 (2014) 3406–3412, https://doi.org/10.1007/s11434-014-0439-7.

[57] Q. Qin, Y. Liu, X. Li, T. Sun, Y. Xu, Enhanced heterogeneous Fenton-like degradation of methylene blue by reduced CuFe2O4, RSC Adv. 8 (2018) 1071–1077, https://doi.org/10.1039/c7ra12488k.

[58] Q. Liao, J. Sun, L. Gao, Degradation of phenol by heterogeneous Fenton reaction using multi-walled carbon nanotube supported Fe2O3 catalysts, Colloids Surfaces A Physicochem. Eng. Asp. 345 (2009) 95–100, https://doi.org/10.1016/j.colsurfa.2009.04.037.

[59] J.H. Ramirez, C.A. Costa, L.M. Madeira, Experimental design to optimize the degradation of the synthetic dye Orange II using Fenton's reagent, Catal. Today 107–108 (2005) 68–76, https://doi.org/10.1016/j.cattod.2005.07.060.

[60] V. Singh, J. Singh, P. Srivastava, Synthesis and characterization of Acacia gum–Fe0Np–silica nanocomposite: an efficient Fenton-like catalyst for the degradation of Remazol Brilliant Violet dye, Appl. Nanosci. 8 (2018) 793–810, https://doi.org/10.1007/s13204-018-0732-x.

[61] M. Delnavaz, J. Farahbakhsh, S.S. Mahdian, Photodegradation of reactive blue 19 dye using magnetic nanophotocatalyst α-Fe2O3/WO3: a comparison study of α-Fe2O3/WO3 and WO3/NaOH, Water Sci. Eng. 14 (2021) 119–128, https://doi.org/10.1016/j.wse.2021.06.007.
[62] Y. Li, Z. Li, Y. Xia, H. Li, J. Shi, A. Zhang, H. Huo, S. Tan, L. Gao, Fabrication of ternary AgBr/BiPO4/g-C3N4 heterostructure with dual Z-scheme and its visible light photocatalytic activity for Reactive Blue 19, Environ. Res. 192 (2021), 110260, https://doi.org/10.1016/j.envres.2020.110260.
[63] H. Xia, H. Zhuang, D. Xiao, T. Zhang, Photocatalytic activity of La3+/S/TiO2 photocatalyst under visible light, J. Alloys Compd. 465 (2008) 328–332, https://doi.org/10.1016/j.jallcom.2007.10.083.
[64] P. Dhiman, T. Mehta, A. Kumar, G. Sharma, M. Naushad, T. Ahamad, G.T. Mola, Mg0.5NixZn0.5-xFe2O4 spinel as a sustainable magnetic nano-photocatalyst with dopant driven band shifting and reduced recombination for visible and solar degradation of Reactive Blue-19, Adv. Powder Technol. 31 (2020) 4585–4597, https://doi.org/10.1016/j.apt.2020.10.010.
[65] E. Hass Caetano Lacerda, F.C. Monteiro, J.R. Kloss, S.T. Fujiwara, Bentonite clay modified with Nb2O5: an efficient and reused photocatalyst for the degradation of reactive textile dye, J. Photochem. Photobiol. Chem. 388 (2020), https://doi.org/10.1016/j.jphotochem.2019.112084.
[66] I. Bibi, S. Kamal, Z. Abbas, S. Atta, F. Majid, K. Jilani, A.I. Hussain, A. Kamal, S. Nouren, A. Abbas, A new approach of photocatalytic degradation of remazol brilliant blue by environment friendly fabricated zinc oxide nanoparticle, Int. J. Environ. Sci. Technol. 17 (2020) 1765–1772, https://doi.org/10.1007/s13762-019-02586-y.
[67] S. Zhang, M. Sun, T. Hedtke, A. Deshmukh, X. Zhou, S. Weon, M. Elimelech, J.H. Kim, Mechanism of heterogeneous Fenton reaction kinetics enhancement under nanoscale spatial confinement, Environ. Sci. Technol. 54 (2020) 10868–10875, https://doi.org/10.1021/acs.est.0c02192.
[68] C.K. Duesterberg, S.E. Mylon, T.D. Waite, pH effects on iron-catalyzed oxidation using Fenton's reagent, Environ. Sci. Technol. 42 (2008) 8522–8527, https://doi.org/10.1021/es801720d.
[69] Y. Yin, Y. Ren, J. Lu, W. Zhang, C. Shan, M. Hua, L. Lv, B. Pan, The nature and catalytic reactivity of UiO-66 supported Fe3O4 nanoparticles provide new insights into Fe-Zr dual active centers in Fenton-like reactions, Appl. Catal. B Environ. 286 (2021), https://doi.org/10.1016/j.apcatb.2021.119943.
[70] M. Aghayi-Anaraki, V. Safarifard, Fe3O4@MOF Magnetic Nanocomposites: Synthesis and Applications, 2020, https://doi.org/10.1002/ejic.202000012.
[71] H. Niu, Y. Zheng, S. Wang, L. Zhao, S. Yang, Y. Cai, Continuous generation of hydroxyl radicals for highly efficient elimination of chlorophenols and phenols catalyzed by heterogeneous Fenton-like catalysts yolk/shell Pd@Fe3O4@metal organic frameworks, J. Hazard Mater. 346 (2018) 174–183, https://doi.org/10.1016/j.jhazmat.2017.12.027.
[72] Z. dong Fang, K. Zhang, J. Liu, J. yu Fan, Z. wei Zhao, Fenton-like oxidation of azo dye in aqueous solution using magnetic Fe3O4-MnO2 nanocomposites as catalysts, Water Sci. Eng. 10 (2017) 326–333, https://doi.org/10.1016/j.wse.2017.10.005.